



Boundary-layer transition delay using free-stream vortex generators

André Weingärtner¹ , Zhuxuan Cui¹, Imge Yigili¹ and Jens H.M. Fransson¹ 

¹FLOW Department Engineering Mechanics, KTH Royal Institute of Technology, Stockholm, Sweden

Corresponding author: Jens H.M. Fransson, jensf@kth.se

(Received 14 November 2024; revised 5 March 2025; accepted 25 March 2025)

Delaying the laminar–turbulent transition of a boundary layer reduces the skin-friction drag and can thereby increase the efficiency of any aerodynamic device. A passive control strategy that has reaped success in transition delay is the introduction of boundary layer streaks. Surface-mounted vortex generators have been found to feature an unstable region right behind the devices, which can be fatal in flow control if transition is triggered, leading to an increase in drag with respect to the reference case without devices. In a previous proof of concept study, numerical simulations were employed to place artificial vortices in the free stream that interact with the boundary layer and accomplish transition delay. In the current study, we present experimental results showing the feasibility of generating free-stream vortices that interact with the boundary layer, creating high- and low-speed boundary layer streaks. This type of streaky base flow can act as stabilizing if introduced properly. We confirm the success of our flow control approach by artificially introducing two-dimensional disturbances that are strongly attenuated in the presence of streaks, leading to a transition delay with respect to the reference case of approximately 40 %.

Key words: boundary layer control, boundary layer stability, drag reduction

1. Introduction

In low-turbulence environments, the two-dimensional boundary layer transition process from laminar to turbulent state is dominated by Tollmien–Schlichting (TS) waves, i.e. two-dimensional waves that are unstable in a particular region of the (Reynolds number, frequency)-parameter space. Such TS waves were predicted theoretically by Tollmien (1929) and Schlichting (1933), and later confirmed experimentally by Schubauer &



Skramstad (1947). In numerous engineering applications, it is of interest to be able to control this transition scenario.

Promoting transition is, for instance, of interest in weakly separated flows since a turbulent boundary layer is more resistant to separation and can make the flow stay attached to the surface, reducing the pressure drag (Pope 2000). Furthermore, a turbulent boundary layer is preferred when increased mixing or heat transfer to the wall is desired. This type of control is, however, relatively easy to obtain since it can be accomplished by tripping the boundary layer with some roughness, tripping tape, or large-scale surface-mounted vortex generators. Delaying transition, on the other hand, is significantly more challenging. The advantages of a prolonged laminar region of a boundary layer flow can, for example, be decreased skin-friction drag or alleviated thermal losses to the wall.

One efficient way to dampen the growth of TS waves is to modulate the mean flow with stable streamwise streaks of alternating high and low speeds, as first shown experimentally by Kachanov & Tararykin (1987). They employed continuous suction and blowing from streamwise slots to achieve a streaky base flow, and were able to show decreased TS wave growth rates with maximum streak amplitudes of about 5%. Other early experimental works where the boundary-layer interaction of artificially generated TS waves with streamwise streaks were studied are, for instance, Tani & Komoda (1962) and Bakchinov *et al.* (1995). In Tani & Komoda (1962), two-dimensional wings were mounted periodically in the free stream using piano wires. The tip vortices from each wing interacted with the boundary layer, resulting in a weakly modulated boundary layer flow of a maximum streak amplitude of about 7%. Bakchinov *et al.* (1995) instead used streamwise elongated rectangular blocks to create alternating high and low speed streaks and obtained a maximum streak amplitude of approximately 15%. All of the above studies reported a stronger amplification of TS waves in the high-speed streak as compared to the low-speed streak, which is counterintuitive from a two-dimensional stability point of view since high- and low-speed streaks are associated with a lower and higher local shape factors, respectively. However, in only one of the above studies was an overall damping effect of TS waves reported, but none showed any indication of transition delay.

In a simplified numerical investigation using linear stability analysis, it was shown that the decisive component in the observed stabilization mechanism is the spanwise velocity gradients (SVGs) in the mean flow (Cossu & Brandt 2002, 2004). The SVGs lead to an additional kinetic disturbance energy production term with respect to the two-dimensional case, which turns out to be of negative sign, causing a stabilization of the boundary layer. The extra term is $-\overline{uw}$ acting on $\partial U/\partial z$, where the latter term is the one that can be influenced. Here, \overline{uw} is the covariance of the streamwise and spanwise velocity components, U is the streamwise mean velocity, and z is the spanwise coordinate. Fransson *et al.* (2005) confirmed the alleviated TS wave growth in wind-tunnel experiments, generating the streaks through a spanwise array of cylindrical roughness elements. Finally, Fransson *et al.* (2006) showed that the transition to turbulence can, in fact, be delayed using this mechanism.

In subsequent studies, various ways to generate SVGs in experiments were investigated. This can be done either actively or passively. Passive flow control for transition delay is appealing for two reasons: it acts without adding any energy to the control system since it utilizes the existing energy in the flow, and it can easily be installed in real flow applications without adding any sensitive electronics that can be damaged in harsh environments. A passive control strategy that has been shown to be successful in many investigations is the introduction of spanwise mean velocity gradients inside the boundary layer, no matter how these gradients are accomplished as long as they are smooth and steady.

Active approaches, such as discrete suction (Sattarzadeh & Fransson 2017), pair of oblique waves (Sattarzadeh & Fransson 2016), plasma actuator vortex generators (Barckmann *et al.* 2015) or rotating cylindrical roughness elements (Römer *et al.* 2023), were shown to be successful, but passive techniques have clear advantages. The previously mentioned static cylindrical roughness elements (Fransson *et al.* 2004, 2005, 2006) have the drawback that for a given aspect ratio, an absolute (global) instability develops in the wake above a certain threshold roughness Reynolds number (Loiseau *et al.* 2014; Weingärtner *et al.* 2023a), leading to destabilization and premature transition to turbulence. Therefore, the achievable amplitude of the generated streaks, which is linked to the roughness Reynolds number, is limited. Another passive approach includes a spanwise array of aerodynamically smooth streamwise-elongated humps (Downs & Fransson 2014) that generate SVGs naturally due to the no-slip condition at the varying wall locations and can likewise delay the transition to turbulence. The same phenomenon can also be found in nature. As shown by Muthuramalingam *et al.* (2020), fish scales can generate alternating high- and low-speed streaks that are able to prolong the laminar region of the flow, reducing the overall drag. The method that has proven most effective in laboratory experiments to generate stable high-amplitude streaks is miniature vortex generators (MVGs). That is, MVGs can generate a streaky base flow with large SVGs, which is necessary to accomplish substantial transition delay (Fransson & Talamelli 2012; Shahinfar *et al.* 2012). These blade-type vortex generators are completely submerged in the laminar boundary layer and feature a relatively small unstable wake region, compared to a solid circular roughness element, since flow is let through in between the two blades.

However, in this context, another effect apart from the roughness Reynolds number and the absolutely unstable wake region must be considered. If the streaks themselves exceed a critical amplitude (for a given spanwise wavelength), then they will become susceptible to secondary instabilities of sinuous or varicose type that can break down to a turbulent spot, leading to an earlier inception of turbulence (Andersson *et al.* 2001). This shows that the amplitude of the streaks is a delicate parameter that needs to be tuned carefully. Several experimental studies have been performed aiming to quantify and optimize the effects of MVGs on boundary layer transition. In-depth investigations to examine how the geometrical parameters of the MVGs are related to the generated streaks have been performed by Shahinfar *et al.* (2013) and Sattarzadeh & Fransson (2015), coming up with scaling relations in order to predict the streaks in any given flow configuration. Downs *et al.* (2017) studied the generation and development of streaks in Falkner–Skån pressure gradient boundary layers. Further work was performed by Weingärtner *et al.* (2023b), now aiming to predict the behaviour of the streamwise streaks on the fuselage of an aircraft. They present an MVG design procedure with the ultimate goal of delaying transition during flight. In all cases, the modulation of the flow quickly reaches a maximum and then tends to relax back to the undisturbed Blasius boundary layer with increasing downstream distance, reducing the SVGs and hence also the stabilizing effect. To counter this, Sattarzadeh *et al.* (2014) investigated the possibility of reinforcing the generated streaks by adding a second array of MVGs at some downstream distance from the first array. By re-energizing the streaky base flow, they could show that even further transition delay can be obtained.

In the context of the above studies, two different experimental set-ups should be distinguished: the disturbances (TS waves) are generated either upstream or downstream of the devices that modulate the flow. These two scenarios have the stark difference that in the first case, the disturbances impinge onto the geometry of the vortex generators, which can cause a nonlinear response with strong disturbance amplification. This devastating interaction is bypassed in the latter case, where the streaks already exist when the TS

waves are introduced. Including the interaction is a more realistic scenario since, in natural transition, disturbances can already be present in the flow upstream of the TS wave instability region (e.g. higher-frequency TS waves or free-stream turbulence) that might interact with the devices and grow algebraically. Cylindrical roughness elements are unable to delay transition when the disturbance is generated upstream of the elements, likely because of the large wake region behind an element and the aforementioned absolute instability. Blade-type MVGs, on the other hand, have proven to be successful in delaying transition even if the interaction of TS waves with the geometry is present. A small initial growth of the disturbances is observed right behind the elements, but if designed properly, this is not sufficient to trigger transition to turbulence (e.g. Shahinfar *et al.* 2012). With the goal of finding an efficient vortex generator that does not consist of delicate edges and can be mounted on any surface with ease, Weingärtner (2024) tested slanted wedges with a triangular base as an alternative shape to blade-type MVGs. Although the mean velocity profiles behind the wedge-type vortex generators and the streak amplitude evolution seemed promising, the transition could not be delayed. Further investigation showed that the TS waves impinging onto the geometry were strongly amplified right behind the devices, leading to advanced transition, although the elements by themselves did not trip the flow. Note that the shape was designed in a streamlined way, so there were no clear regions of flow separation in the wake of the devices.

In the experimental study by Sattarzadeh & Fransson (2014), additional regions of instability behind the MVG elements as a result of the interaction of incoming TS waves with the geometry were already suspected, which was investigated in detail by means of direct numerical simulations (DNS) and stability analysis by Siconolfi *et al.* (2015b). They proved the existence of an absolute instability in the near wake of the MVG blades, which is likely the origin of the initial disturbance growth and destabilization observed in all previous investigations that employ MVGs. This underlines that the ideal case would be to introduce vortices without any physical device that disturbs the boundary layer at all, which can be performed only in a fictive numerical simulation without moving to active control. Siconolfi *et al.* (2015a) performed DNS and placed free-stream vortices above a laminar boundary layer to generate the streaky base flow farther downstream. Their simulations were partly based on the successful MVG case C01 of Shahinfar *et al.* (2013) in order to have physically relevant values of the modelled vortices in the DNS. Varying the location and strength of the vortices, they show how the mean flow is modulated in the different cases, and prove that damping of disturbances and transition delay is indeed possible using this approach. Martín & Paredes (2017) conducted a numerical study, based on the parameters chosen by Siconolfi *et al.* (2015a), in which vortices are positioned at various heights above the wall on a flat plate while keeping a fixed maximum streak amplitude (20 %) inside the boundary layer by varying the vortex circulation. They reported that when the vortices are placed farther from the wall, the boundary layer is perturbed in a smoother way, but the modulation takes place further downstream. They identified an optimum wall-normal distance for the attenuation of TS waves of $2.18\delta_{99}$ at their employed streamwise location for vortex generation of 52 mm from the leading edge (similar to Siconolfi *et al.* 2015a).

Szabó *et al.* (2024) recently performed stability analyses of MVGs using computationally less expensive approaches (e^N method), therefore enabling a large parameter variation of different geometries. In their study, they investigated separately the stabilizing effect of the streaks on the TS waves and the secondary instabilities that the streaks can develop, potentially causing earlier transition. One significant outcome is an improved configuration of the blade-type MVGs used in the experimental studies by Fransson's group at KTH Royal Institute of Technology, Stockholm, aiming for optimal

transition delay. To the present authors' knowledge, this configuration has yet to be tested in an experiment.

In the present investigation, we use free-stream vortex generators (FSVGs) to generate a streaky base flow through vortices outside the boundary layer. This approach builds upon the delta wings previously investigated at KTH in the master's thesis works by Lozano (2017) and Cui (2023). The data presented in this paper originate from the latter study. The goals of the study are twofold. First, we want to confirm experimentally the results of Siconolfi *et al.* (2015*a*), where free-stream vortices were used to stabilize the boundary layer in a numerical simulation. Second, we aim to explore methods to generate a streaky base flow while keeping the boundary layer as undisturbed as possible. Using FSVGs, it is likely possible to avoid (or significantly reduce) an absolute instability in the boundary layer (Siconolfi *et al.* 2015*b*), and hence to minimize the initial disturbance growth due to the interaction between incoming TS waves and the geometry.

The paper is structured as follows. In § 2, the experimental set-up and the FSVGs are described. This is followed in § 3 by a characterization of the reference base flow and the disturbance growth of TS waves that is used for comparisons with modulated base flows. In § 4, the modulated base flows using different FSVG configurations are quantified (§ 4.1), and the amplifications of TS waves, in both the linear (§ 4.2) and nonlinear (§ 4.3) regimes, are reported. Finally, in § 5, we summarize and conclude our findings.

2. Experimental set-up

2.1. Experimental facility and measurement technique

The measurements were performed in the BL wind tunnel at KTH. The test section has cross-sectional area $0.5 \times 0.75 \text{ m}^2$ and length 4.2 m. The axial fan (DC 15 kW) can produce airflow in the empty test section with speed up to 48 m s^{-1} , and the cooling system of the wind tunnel is capable of maintaining a constant temperature in the test section within $\pm 0.07 \text{ }^\circ\text{C}$. The streamwise turbulence intensity in the test section is less than 0.04 % in the core, with similar values for the cross-flow turbulence intensities at nominal speed 25 m s^{-1} (cf. Lindgren & Johansson 2002).

The experiments were carried out over a 3.5 m long flat plate with a superelliptical leading edge according to

$$\left(\frac{x}{a}\right)^m + \left(\frac{y}{b}\right)^n = 1, \quad (2.1)$$

where the aspect ratio AR ($= a/b$) is 20 : 1, with $a = 200 \text{ mm}$, and the exponents $(m, n) = (2.3, 1.9)$. The plate is positioned vertically in the test section to achieve the best spanwise homogeneity in the flow. With the installation of a trailing flap along with the adjustable side wall of the test section, a zero pressure gradient boundary layer flow with a relatively short pressure gradient region close to the leading edge was obtained. The free-stream velocity in the current experiments was kept constant at $U_\infty = 5.9 \text{ m s}^{-1}$, measured above the plate sufficiently far downstream of the leading edge. A sketch of the experimental set-up is shown in figure 1.

Hot-wire anemometry was employed throughout the campaign to measure time-resolved streamwise velocity signals along the flat plate. A single-sensor hot-wire probe operating in constant temperature mode was manufactured in-house, employing Wollaston wire composed of platinum with 10 % rhodium. The wire, of diameter $2.5 \text{ }\mu\text{m}$ and length 0.5 mm, was fully etched before being soldered to the hot-wire prongs. Data were collected using a 16-bit NI USB-6215 DAQ system at sampling frequency 5 kHz. The probe was

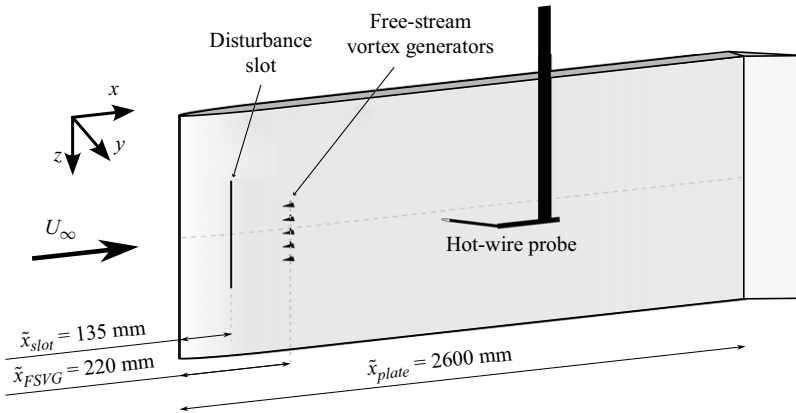


Figure 1. Sketch of the experimental set-up. Quantities \tilde{x} denote distances from the leading edge; otherwise, the origin of the applied coordinate system for the measurements is the trailing edge of the FSVGs (cf. figure 2).

calibrated in the free stream inside the tunnel against the dynamic pressure obtained from a Prandtl tube connected to a Furness FCO560 differential manometer.

The TS waves were introduced by periodic blowing and suction at the wall through a spanwise slot at $\tilde{x} = 135$ mm from the leading edge. The sinusoidal signal is generated using a function generator and supplied to an audio amplifier driving a loudspeaker, which is connected to the slot through tightly sealed silicon hoses. The amplitude of the disturbances from the slot can be quantified by measuring the AC output voltage from the amplifier to the loudspeaker.

Due to the viscous nature of the boundary layer instability, we here introduce the standard non-dimensional frequency F according to

$$F = 2\pi f \nu \times 10^6 / U_\infty^2, \quad (2.2)$$

where f is the dimensional frequency in Hz, and ν is the kinematic viscosity. For the current tests, a constant value $F = 175$ was employed throughout. For the chosen U_∞ , this positions branch II of the neutral stability curve at the centre of the measurement domain, allowing good resolution in the measurements for the transition region, which is expected to occur after branch II. The study of only one TS wave frequency is warranted since many studies have shown that if a modulated base flow is efficient in delaying transition for one TS wave frequency, then it is also efficient for others (cf. Shahinfar *et al.* 2012). In addition, from the stability analysis study by Siconolfi *et al.* (2015b), it is evident that with a streaky base flow, the neutral stability curve of the reference Blasius boundary layer will shift downstream at the same time as it is quenched towards lower frequencies as the streak amplitude increases. All this supports our decision to present only one TS wave frequency, since the rest is all about streaky base flow optimization; with one frequency, we can conclude that the stabilization is successful and that we can obtain transition delay. Testing more than one frequency is not warranted due to the time consumption. Considering all the cross-sectional planes that need to be taken in order to integrate the base flow modulation and the TS wave amplitude accurately, this would not add any extra value to the study.

2.2. The FSVGs

The FSVGs are utilized to create SVGs in the boundary layer. The advantage of this type of vortex generator over the wall-mounted devices is their significantly reduced influence on

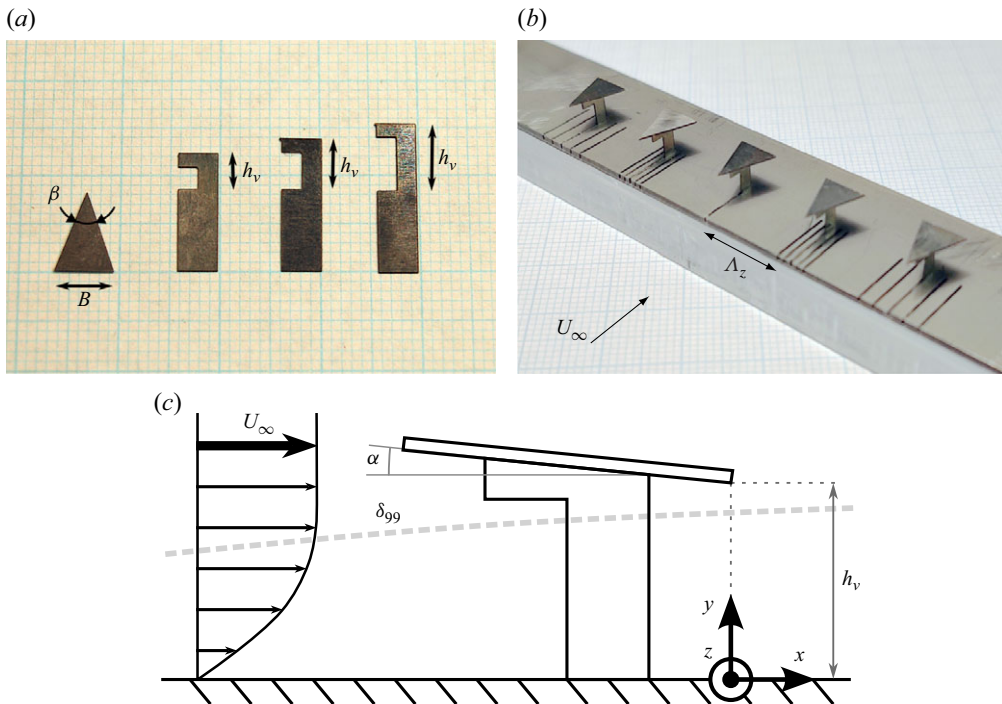


Figure 2. (a) The FSVGs consist of a triangular delta wing and a separate leg. (b) The assembled devices, mounted in a spanwise array. The streamwise cuts allow us to vary the FSVG spacing (however, not used here). The rail was then flush-mounted in a slot in the plate. (c) A side-view sketch of the set-up and the employed coordinate system.

the boundary layer. The vortex pairs generated by the FSVGs can have a higher intensity as they develop for a longer time in the free stream. In the current experiments, the FSVGs are made of two parts, triangular delta wings and separate legs, which are shown in [figure 2\(a\)](#). The delta wings are isosceles triangles with base length $B = 6$ mm and sweep angle $\beta = 40^\circ$. The legs have a trapezoidal shape with a cut-out to minimize the wake effect. Both parts are cut from stainless steel sheets using electrical discharge manufacturing, and glued together using a specifically designed device to ensure that the angle is close to the intended value ([Lozano 2017](#)). The thicknesses of the legs and the delta wings are 0.15 mm and 0.3 mm, respectively. The FSVGs are then installed into small sliding blocks that are placed on a rail to adjust the spacing (Λ_z) between them. A plate to cover this rail is installed, and the assembly is inserted into the slot on the flat plate. The mounted FSVG devices including the cover plate are shown in a photo in [figure 2\(b\)](#). Five FSVGs were mounted on the flat plate, and all measurements were performed behind the central element of the array in order to achieve quasi-two-dimensional conditions. Once installed, a single plane measurement covering the wake of all five elements was performed in order to identify flawed FSVGs that might not have been installed or manufactured at the correct angle. These devices were then re-mounted or replaced iteratively, ensuring that all FSVGs behave similarly. More information on the manufacturing and mounting process is given in [Cui \(2023\)](#). A side-view sketch of the set-up is shown in [figure 2\(c\)](#), where the angle of attack (α) and the height of the vortex generators (h_v) and the boundary layer thickness (δ_{99}) are introduced, as well as the origin of the coordinate system for the measurements.

Case	α (deg.)	h_v/δ_{99}	h_v (mm)	Colour (from figure 6 onwards)
C0	0 ± 0.1	1.4	5.25	●
C1	0.5 ± 0.1	1.0	3.73	■
C2	0.5 ± 0.1	1.4	5.25	▲
C3	1.0 ± 0.1	1.4	5.25	▼
C4	2.0 ± 0.1	1.9	7.00	◆

Table 1. FSVG configurations and geometrical parameters. The spanwise distance between the FSVGs was constant at $\Lambda_z = 14$ mm in all cases.

2.3. Investigated FSVG parameters

The abundant number of FSVG parameters makes a complete parameter variation study impossible in an isolated work, meaning that some parameters were locked *a priori* to focus on what we believe are the most relevant for our purpose. Apart from the FSVG design parameters β , B , h_v , Λ_z , α introduced in figure 2, there are two other parameters influencing the strength of the vortices and the interaction with the boundary layer. These parameters are U_∞ and δ_{99} , which are directly related to each other since the location of the FSVGs in the streamwise direction (\tilde{x}_{FSVG}) is locked (see figure 1). In the present study, β , B , Λ_z , U_∞ and hence δ_{99} are kept constant. Our focus has been on the influence of α and h_v on the boundary layer interaction leading to the desired boundary layer modulation. The separate leg was kept the same except for its height above the wall, i.e. varied through h_v .

Based on the range of vortex heights h_v investigated by Siconolfi *et al.* (2015b), which varied from $1\delta_{99}$ to $2.5\delta_{99}$, three h_v values have been selected. On the other hand, the range of α has been chosen such that streaks with too-high amplitudes are avoided, as angle of attack 3° with free-stream velocity 4 m s^{-1} has been observed to generate streaks of 70 % amplitude in the work of Lozano (2017). The spacing between the FSVGs, Λ_z , has been set to 14 mm, based on previous research by Shahinfar *et al.* (2012), Siconolfi *et al.* (2015a) and Lozano (2017). The different FSVG cases investigated here are summarized in table 1.

3. Reference base flow and TS wave characterization

In this section, we characterize the reference two-dimensional boundary layer flow and present the quality of the generated TS waves. Measured laminar velocity profiles at various downstream and spanwise locations are shown in figure 3(a) and compared with the numerical Blasius solution, where δ_1 is the corresponding boundary layer displacement thickness, and U_∞ is the local free-stream velocity of the measured profile. Profiles are shown in the whole range of interest, where the range of the wind-tunnel traverse limits the streamwise distance. Results demonstrate good agreement with the Blasius theory, confirming that there is a negligible pressure gradient along the length of the plate. Figure 3(b) shows the streamwise evolution of δ_1 and the momentum thickness (δ_2) of the boundary layer along with the shape factor (H_{12}). As expected, the non-zero pressure gradient in the leading-edge region of the plate gives rise to a virtual origin \tilde{x}_0 of the boundary layer, which is determined to be $\tilde{x}_0 = 5.5$ mm, i.e. \tilde{x}_0 is located 5.5 mm downstream of the leading edge. One procedure to determine \tilde{x}_0 (as applied here) is to fit the theoretical curves of $\delta_1(x)$ and $\delta_2(x)$ with a variable offset \tilde{x}_0 to the experimental data ($\delta_1 = 1.72\sqrt{(\tilde{x}_{FSVG} + x - \tilde{x}_0)\nu/U_\infty}$, and similarly for δ_2 , with factor 0.664 instead). The two \tilde{x}_0 values are then averaged. Recall that here, $x = 0$ mm corresponds to the location

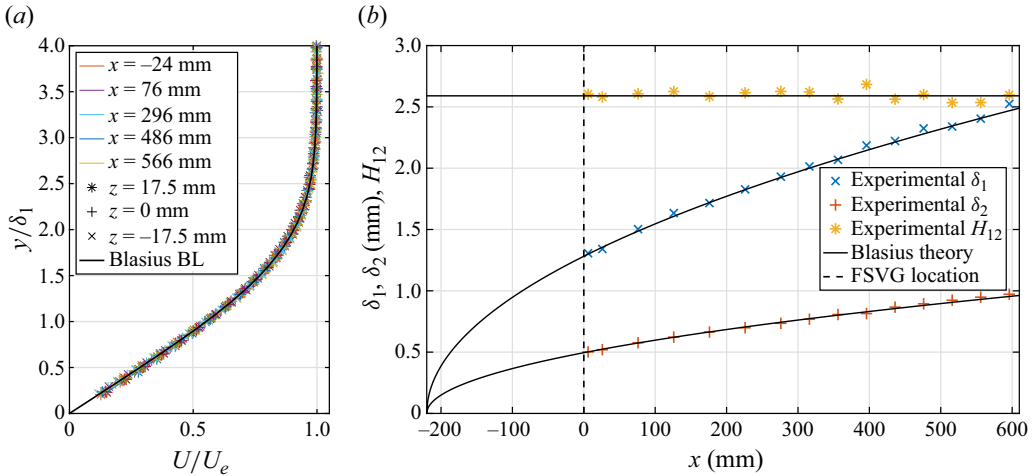


Figure 3. Reference two-dimensional base flow case. (a) Experimental wall-normal mean velocity profiles for different streamwise and spanwise locations. The solid line corresponds to the Blasius solution. (b) Dimensional boundary layer displacement and momentum thicknesses along with the shape factor. See the text for the theoretical curve fitting and determination of the virtual origin from the leading edge. Data are presented in the streamwise extent of Re_δ from 294 to 568.

of the FSVGs, i.e. 220 mm downstream of the leading edge of the plate. In this section, we characterize the reference two-dimensional boundary layer flow and present the quality of the generated TS waves.

Next, the generated TS wave ($F = 175$) in the reference boundary layer is reported. To show the quality of the experimental set-up and the measurements, a TS wave amplitude (A_{TS}) distribution in the wall-normal direction is shown in figure 4(a), at a streamwise location corresponding to the centre in between branch I and branch II of the neutral stability curve. The wall-normal amplitude distribution is compared with linear stability theory (solid line in figure 4a), showing good agreement, which is in line with previous investigations in this facility.

In accordance with Fransson *et al.* (2005), we here define a double integral TS wave amplitude measure for each streamwise location as

$$A_{TS}^{int}(x) = \int_{-1/2}^{1/2} \int_0^{\eta^*} \frac{A_{TS}(x, y, z)}{U_\infty} d\eta d\zeta, \quad (3.1)$$

where $\eta = y/\delta$ and $\zeta = z/\Lambda_z$. That is, the amplitude is integrated over a cross-sectional plane at each streamwise station. In the wall-normal direction, the integration limits are from the wall to the truncated value $\eta^* = 9$ in the free stream, and in the spanwise direction, they are over the separated distance between two subsequent FSVGs, i.e. over one spanwise wavelength Λ_z . Here, $\delta = \sqrt{x\nu/U_\infty}$ is the boundary layer scale, and $\Lambda_z = 14$ mm. This measure is, in particular, important when comparing TS wave amplitude growth curves in various three-dimensional modulated base flows with the reference baseline case. Since the TS wave amplitude distribution depends on the base flow, it will quickly adapt to the modulated boundary layer and in turn become modulated. Hence a surface integral measure of the TS wave is the only way to accomplish a fair comparison between two- and three-dimensional boundary layer flow, which will be done in the next section.

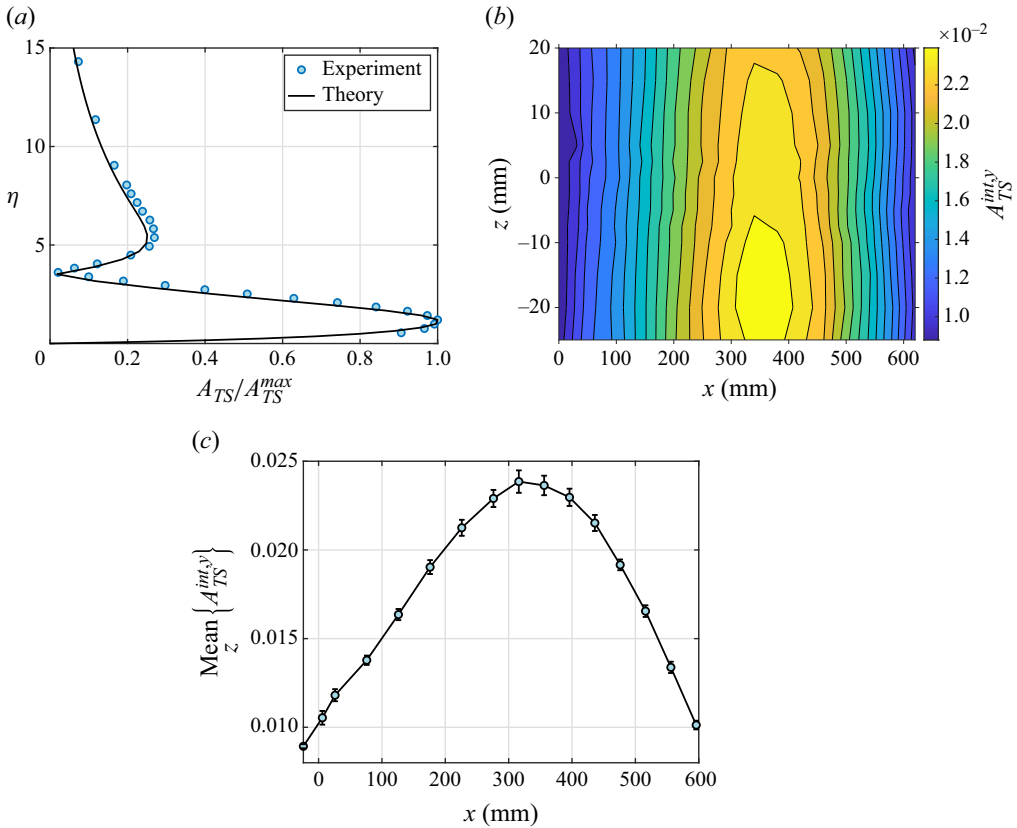


Figure 4. The TS wave characterization for the current base flow. (a) Sample of a TS wave amplitude profile in the wall-normal direction, at $(x, z) = (76, 0)76, 0$ mm and for $F = 175$. The theoretical profile is normalized with the maximum value of the experimental data. (b) Wall-normal integrated amplitude measure $A_{TS}^{int,y}(x, z)$ in the measurement region. (c) Spanwise-averaged TS wave growth curve from (b) is shown. For error bars, see text.

Figure 4(b) further illustrates the quality of the experiments by plotting $A_{TS}^{int,y}$ of the reference case in the xz -plane, where $A_{TS}^{int,y}$ is obtained by integrating the amplitude distribution (A_{TS}/U_∞) only in the wall-normal direction (cf. (3.1)). The TS waves are shown to be close to two-dimensional despite using a more sensitive integral measure. The spanwise-averaged growth curve is plotted in figure 4(c), where the error bars correspond to the root mean square (r.m.s.) value from 13 different spanwise locations over a range of 35 mm ($= 2.5\Lambda_z$). Branch II, with maximum amplitude, is seen to be located at approximately $x = 320$ mm (downstream of the location where the FSVGs can be mounted), which agrees well with linear stability theory. It is worth noting that if one uses a so-called maximum measure of the TS wave amplitude instead (i.e. maximum value in $A_{TS}(y)$), which is a common way to illustrate the streamwise evolution of the TS wave amplitude, then the error bars will approximately be halved.

4. The TS wave amplification in FSVG-modulated base flows

4.1. Mean flow modulation and quantification

In this subsection, the effect of different FSVG configurations on the mean flow is investigated. It is worth noting that due to the natural growth of the laminar boundary layer,

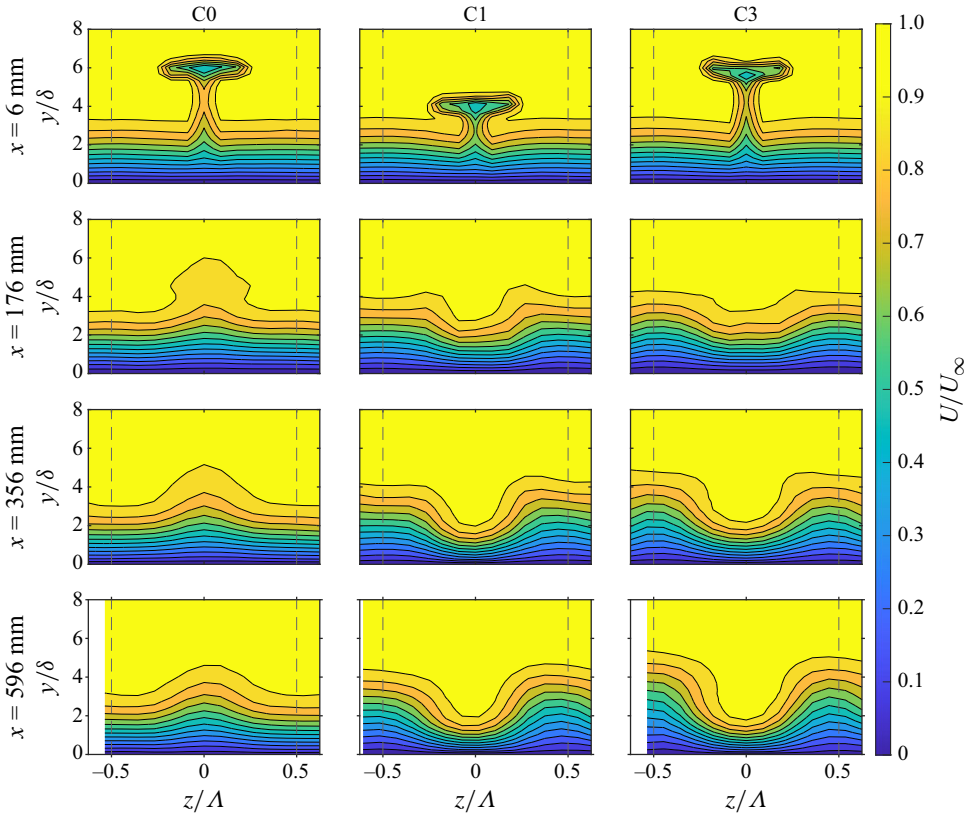


Figure 5. Streamwise mean velocity fields for C0, C1 and C3 (columns) at various downstream locations (rows). Dashed lines at $z/\Lambda = \pm 0.5$ indicate integration limits in (4.1).

even an FSVG with a delta wing of a geometrical angle of zero degrees will experience some effective angle of attack. The effective angle will always be positive, and as long as it is positioned outside the boundary layer, independent of the distance to the wall. It will, however, change with the streamwise location. Using the Blasius similarity solution for the wall-normal velocity component, the displacement velocity at the location of the FSVGs can be estimated to be 0.018 m s^{-1} , giving induced angle of attack 0.17° . It is worth mentioning that this angle is not far from the estimated manufacturing uncertainty $\pm 0.1^\circ$ as given in table 1.

The positive angle of attack of the delta wings results in a difference in pressure between the upper (suction) and lower (pressure) sides, which leads to the generation of leading-edge vortices, and hence to the existence of streamwise vorticity in the flow. Now, the presence of a counter-rotating vortex pair behind the delta wing results in wall-normal transport of fluid, with a common downwash on the centreline behind the delta wing that pushes high-momentum fluid towards the surface. At the same time, the vortex upwash, on the sides, tends to lift up low-momentum fluid towards the edge of the boundary layer. Hence streamwise streaks of alternating high and low speed are generated, with a single high-speed streak in line with the element, and two low-speed streaks on the sides.

Figure 5 shows the streamwise mean velocity in cross-sectional planes measured at various downstream locations behind the FSVG array for three out of the total five cases (cf. table 1). Case C0 (left-hand column of figure 5), featuring geometric angle 0° , does

not show a high-speed streak behind the element. Instead, a central low-speed streak is generated that decays with the downstream distance. This indicates that the production of streamwise vorticity due to the induced angle of attack is negligible, and instead the no-slip condition on the delta wing and subsequent wake behind it fully dominates. Another conclusion that can be drawn from C0 is that the angle of attack is in fact close to the intended value 0° , making it likely that the other cases also feature the angle of attack that they are designed to have.

All cases with a positive angle of attack (C1–C4) show the generation of a central high-speed streak as per the aforementioned mechanism. The vortices slowly enter the boundary layer because of their slight downward trajectory as a result of the positive angle of attack, but also due to the boundary layer's natural growth. The outcome is a high-speed streak in the centre, and two low-speed streaks on the sides. As expected, the formation of the high-speed streak inside the boundary layer begins earlier, with decreased height of the FSVGs above the wall since the vortices will interact with the boundary layer earlier. Furthermore, a larger angle of attack results in stronger vortices, and steepens somewhat the trajectory of the vortices towards the wall, resulting in a stronger and earlier impact on the boundary layer.

To quantify the modulation of the mean flow in a single non-dimensional quantity, the streak amplitude can be calculated. Various definitions can be found in the literature, but one that has proven to be meaningful in the context of attenuation of disturbances in the flow is the integrated streak amplitude, introduced by Shahinfar *et al.* (2013):

$$A_{ST}^{int}(x) = \int_{-1/2}^{1/2} \int_0^{\eta^*} \frac{|U(x, y, z) - U^z(x, y)|}{U_\infty} d\eta d\zeta. \quad (4.1)$$

Here, the non-dimensional variables are similar to the integrated TS wave amplitude definition (3.1) and U^z is the spanwise-averaged velocity profile. Note that A_{ST}^{int} is independent of the chosen η^* as long as it is sufficiently far above h_v , where the integrand is zero. Other definitions that utilize the normalized difference between the maximum and minimum velocities in the span (e.g. Andersson *et al.* 2001) have the drawback that they do not include a spanwise length scale. Hence information about the mean flow gradient $\partial U/\partial z$, which is the quantity responsible for the boundary layer stabilization (Cossu & Brandt 2004), is not included. Results for the integrated streak amplitude (4.1) of the investigated FSVG cases are shown in figure 6. Consistent with previous investigations, the streak amplitude grows as the induced velocity of the vortices causes the generation of streamwise streaks in the flow. The cases C0 and C1 show initially high values right behind the FSVGs, but as can be seen in figure 5, this is due to the no-slip wake effect of the geometry, which will slowly recover in the downstream direction (C0). In C1, the wake recovery is accelerated by the vortices, which not only neutralize the wake, but push high-momentum fluid towards the wall, creating a high-speed streak inside the boundary layer.

Compared to the streak amplitude evolution of classical wall-mounted MVGs in zero pressure gradient flows (e.g. Shahinfar *et al.* 2013; Sattarzadeh & Fransson 2015), the streak amplitude due to the FSVGs grows more slowly and reaches a peak significantly later. In fact, the peak was not resolved in any of the investigated cases due to limits in traversing distance. Only in C1 can a peak be discerned in the most downstream region, while C2–C4 continue to grow. This observation is consistent with Siconolfi *et al.* (2015b), using free-stream vortices in DNS to generate a streaky base flow. A comparison is attempted in Appendix A, although several parameters differ. Nonetheless, qualitative agreement of the data can be observed. This discrepancy between MVGs and FSVGs can

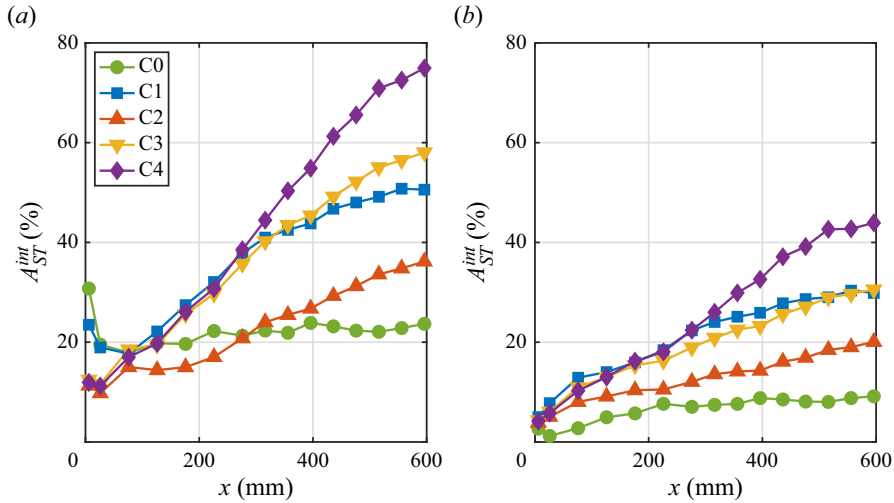


Figure 6. Integrated streak amplitude values for the investigated cases: (a) full streak amplitude, performing the η integral in (4.1) along the full wall-normal length ($\eta^* = 9$); (b) inner boundary layer streak amplitude, with integration up to $\eta^* = 2.5 = 0.5 \delta_{99}$.

be explained by the fact that the vortices, being generated and located in the free stream, are sustained for significantly longer due to lower viscous dissipation in that region. Hence they can also modulate the boundary layer for a longer distance.

The streak amplitude is generally significantly higher than the optimal values for transition delay suggested in previous studies. Using blade-type MVGs, Shahinfar *et al.* (2013) found that an integrated streak amplitude of 30% is optimal for transition delay. Even though stable streaks of an amplitude of 60% can be obtained with MVGs (cf. figure 10 of Shahinfar *et al.* 2013), they are not robust against TS waves, and advance the transition location compared to the two-dimensional reference case already from approximately $A_{ST}^{int} = 40\%$ (cf. figure 20 of Shahinfar *et al.* 2013). The present results show that the streaks have amplitudes of up to 75% in C4. But even C1 and C3 feature amplitudes of 50% and 60%, respectively, which according to MVG modulated boundary layer results would correspond to unsuccessful control cases. Nonetheless, all these cases are successful in stabilization and transition delay, as will be shown later in this paper. However, comparing the present data to the free-stream vortex results by Siconolfi *et al.* (2015a), who used a maximum-based streak amplitude definition, the amplitude values appear reasonable and close to the best case in their DNS (see Appendix A). This raises the question of whether the destabilization observed by Shahinfar *et al.* (2013) is indeed due to the excess streak amplitude or rather the disturbance introduced by the MVG geometry. It was shown by Siconolfi *et al.* (2015b) that blade-type MVGs feature an absolute instability in their wake, which is likely more severe for larger and more intrusive geometries, which also generate stronger streaks. This suggests that the wake effect is the leading source of destabilization, rather than the intensity of the streaks.

Another observation can be made when comparing the streak amplitude of case C0 to the MVG cases of e.g. Shahinfar *et al.* (2013). Case C0 features a streak amplitude of more than 20% due to the low-speed streak originating from the device wake. As will be shown in the next subsection, this case gives, however, a very modest damping of the TS waves, although a streak amplitude of 20% is expected to be appropriate for TS wave attenuation (e.g. Shahinfar *et al.* 2013). This can be explained by the fact that the FSVG streaks are located mostly in the outer region of the boundary layer, while the largest amplitude of TS

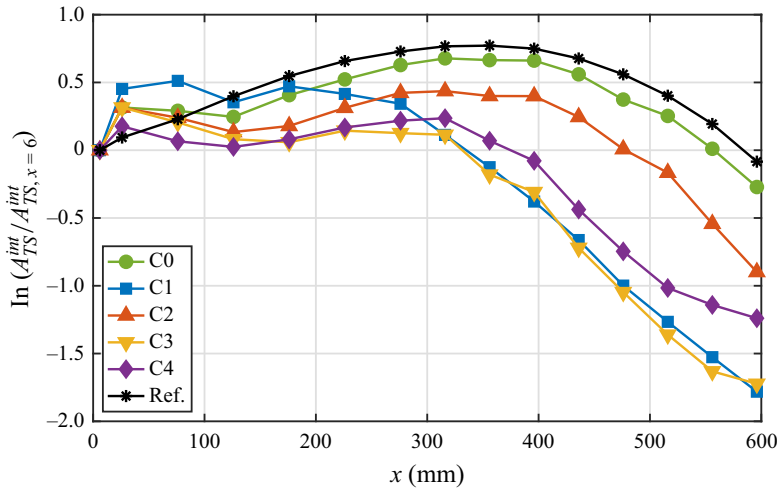


Figure 7. Normalized TS wave amplitude with the downstream distance for the different cases in the linear regime (low disturbance amplitude), $F = 175$.

waves is known to be close to the wall (see figure 4a). Wall-mounted devices, on the other hand, produce streaks (i.e. SVGs) near the surface. Due to the integral definition of the streak amplitude, it contains no information about the wall-normal location of the streaks. As a result, the values of the streak amplitude generated by MVGs and FSVGs are likely not directly comparable when it comes to boundary layer stabilization.

To overcome this apparent discrepancy, the inner boundary layer streak amplitude can be introduced (figure 6b). Here, the wall-normal integral is performed only until $\eta^* = 2.5\delta = 0.5\delta_{99}$ to more accurately represent the effect of the mean-flow modulation on the TS wave. For these integration limits, the values are closer to the proposed optimal value of 30%, while the (almost) ineffective case C0 lacks sufficient inner streak amplitude. However, this quantity has not been calculated for MVG streaks since the streaks are naturally near the wall, so a direct comparison is not possible.

4.2. Stabilization in the linear regime

By ‘linear regime’ here we refer to the fact that disturbance amplitudes are kept sufficiently low, so the assumption of small amplitudes, as used in linear stability theory, is valid. One procedure to guarantee this is to tune the TS wave amplitude to be less than 0.5% at branch II, i.e. $(A_{TS}/U_\infty)_{II} \leq 0.5\%$ (cf. Fransson *et al.* 2005), which was ensured here by iteratively tuning the voltage to the loudspeaker to an appropriate level.

The effect of the various FSVG configurations on the linear TS wave growth curves is shown in figure 7. All values are normalized with their respective first measurement point right behind the FSVGs, i.e. at $x = 6$ mm. The base flow shows the expected TS wave growth curve, featuring growth until $x = 350$ mm (branch II) and decay thereafter. All presented cases with modulated base flow show a reduction in the disturbance amplitude compared to the unmodulated case. The cases C1 and C3 feature the strongest attenuation of TS waves far downstream, while C3 performs better in the close region until approximately $x = 300$ mm. The two cases with the highest streak amplitude, C3 and C4, both feature an inflection point at approximately 550 mm and 500 mm, respectively, which could indicate the onset of a base flow instability due to a too-high streak amplitude. The overall attenuation of C1 and C3 can be quantified by comparing the TS wave amplitude at the most downstream measured location ($x = 596$ mm) giving

$([A_{TS}^{int}]^{3D}/[A_{TS}^{int}]^{2D})_{x=596\text{ mm}} \approx 0.2$, corresponding to a reduction in TS wave amplitude of 80 %.

The initial amplification due to the presence of the FSVGs can be analysed by comparing the second most upstream point in the A_{TS}^{int} evolution in figure 7. It shows that the initial amplification is clearly correlated with the distance of the delta wings to the wall h_v . The case with the devices closest to the wall features the strongest initial growth, while for the case far away, it is marginal. The angle of attack of the delta wing has a negligible influence. However, the initial amplification seems to be harmless at least for the configurations studied here. As will be shown in the next subsection, even the strongest observed initial amplification (C1) is not sufficient to trigger the transition to turbulence prematurely.

In a numerical study, Martín & Paredes (2017) analysed the optimal wall-normal distance of introduced vortices to maximize streak generation and disturbance attenuation. Their parameters, inspired by Siconolfi *et al.* (2015a), included free-stream velocity 7.7 m s^{-1} , and vortex introduction point at 52 mm. They identified an optimal wall-normal distance $h_v = 2.18\delta_{99}$, or 3.4 mm from the wall. Matching these optimal parameters in the present experiment for direct comparison is challenging, if not impossible. Both Siconolfi *et al.* (2015a) and Martín & Paredes (2017) fixed the vortex introduction at $x = 52\text{ mm}$, and in the latter work, the circulation was adjusted to maintain a 20 % maximum streak amplitude. At this location, the boundary layer thickness δ_{99} is only 1.6 mm. Experimental constraints, including precise delta wing mounting, require feasible parameter selection. Studies on passive flow control highlight the importance of both streak amplitude and its streamwise location relative to the neutral stability curve for transition delay. In Siconolfi *et al.* (2015a) (E2) and Martín & Paredes (2017) ($h_v = 2.18$), a 20 % streak amplitude was chosen based on the successful MVG case C01 by Shahinfar *et al.* (2013), with maximum streak locations at $Re_\delta = 726$ and 650, respectively. In the present experiment, $Re_\delta = 567$ for C01, but with a higher streak amplitude ($\sim 25\%$). This lower Re_δ and increased amplitude with respect to the numerical works are favourable, provided that instability does not occur. It is noteworthy that the successful C01 by Shahinfar *et al.* (2013) has a maximum streak amplitude at $Re_\delta \approx 600$. In the experiment, the streak amplitude distribution can be adjusted via delta wing angle of attack, height, and FSVG streamwise position, but neither maximum amplitude nor location can be held constant. Thus the systematic numerical studies cannot be validated directly in experiments, though the reverse is possible.

4.3. Transition delay

It is worth pointing out that even though TS wave attenuation can be accomplished, it is not certain that it can lead to transition delay. In order to test if transition delay is achievable with the given set-up, the amplitude of the loudspeaker was increased in the reference case (i.e. without FSVGs) until transition occurred within the measurement region.

Here, we define the normalized wall-normal integrated energy E^{int} , which is a more appropriate measure as compared to the TS wave amplitude, when analysing high-amplitude disturbance growth due to the broad-band nature of transition and turbulence. This energy measure is defined as

$$E^{int}(x) = \int_{-1/2}^{1/2} \int_0^{\eta^*} \left(\frac{u_{rms}}{U_\infty} \right)^2 d\eta d\zeta, \quad (4.2)$$

where subscript rms indicates the r.m.s. value of the velocity signal, and int refers to wall-normal integration up to $\eta^* = 9$ (similar to the truncated value used in (3.1) and (4.1)).

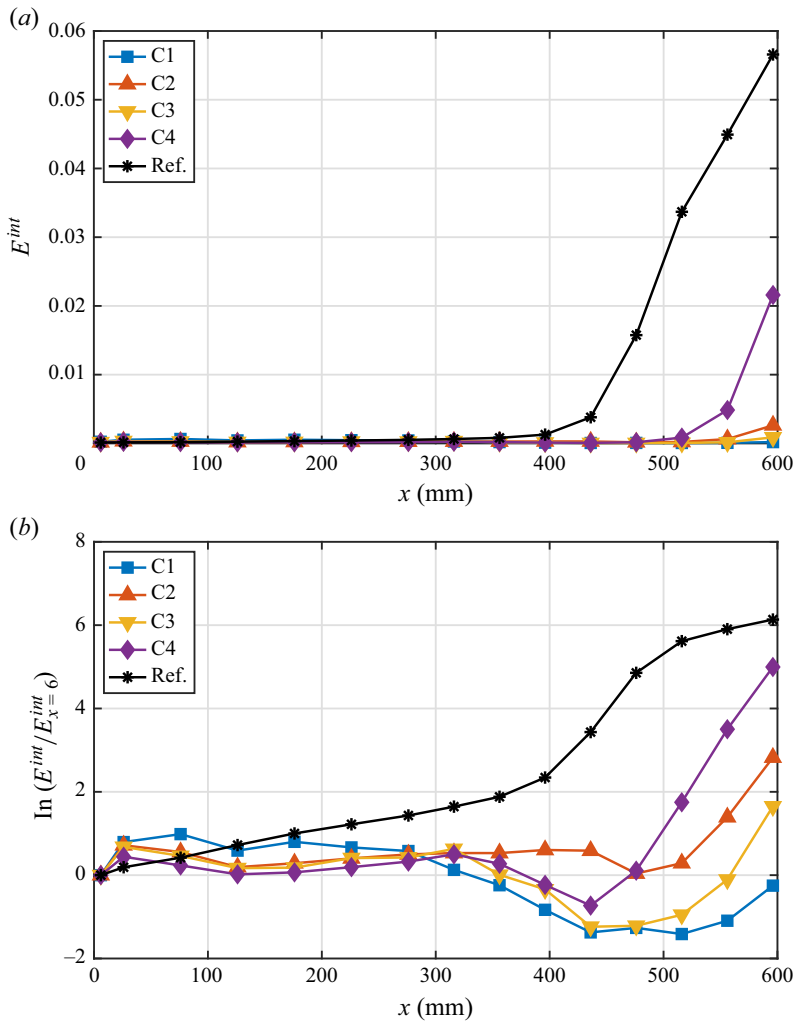


Figure 8. (a) Normalized disturbance energy (4.2) versus the downstream distance for the different cases in the transition case (large disturbance amplitude). (b) Same data as in (a), but log plot and growth curves normalized by corresponding first upstream measured point at $x = 6$ mm.

In figure 8(a), E^{int} is plotted versus the downstream distance for all configurations except C0, which showed a relatively weak damping effect of TS waves in the linear regime. The data show a success of transition to turbulence delay using FSVGs. In the reference, uncontrolled case, one can see that the onset of transition to turbulence takes place at approximately $x = 400$ mm whereafter E^{int} grows sharply. In all the configurations C1–C4, there is a delay in transition, with C1 performing the best. The disturbance energy for C1 at $x = 596$ mm is actually lower than in the first measured upstream location at $x = 6$ mm due to the stabilization. It is noteworthy that at $x = 596$ mm, the energy E^{int} is approximately 500 times larger in the reference case with respect to C1.

In order to separate the data in figure 8(a) and allow for a detailed analysis of the tiny differences in the growth curves, the energy is replotted in figure 8(b) with a log scale and with data normalized with the first upstream measured point. Here, we recall from figure 6 that the streak amplitude overall increases in the following order: C2, C1, C3 and

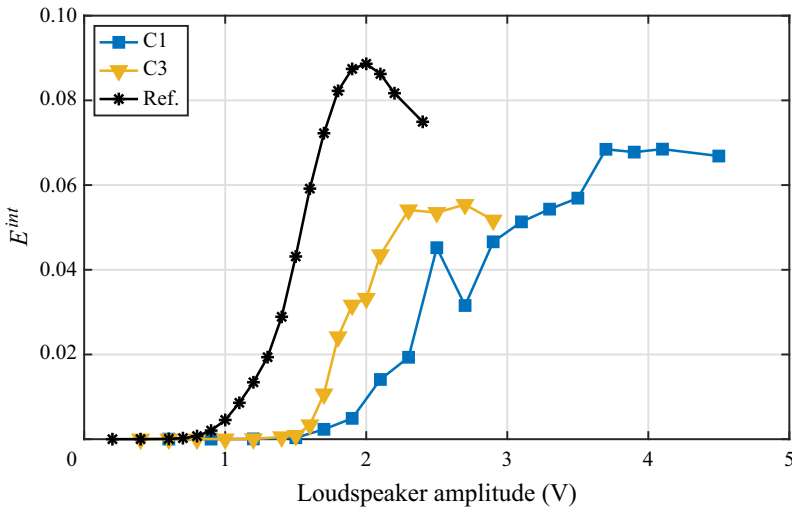


Figure 9. Normalized disturbance energy with increasing voltage supplied to the speaker, leading to a gradual increase in the initial amplitude of the perturbation.

C4. Keeping this in mind when analysing [figure 8\(b\)](#), some conjectures can be made. Case C1 performs better than C2, and it can be argued that the streak amplitude in C2 is below the optimal one for transition delay using FSVGs. Case C3 also performs worse than C1, which might be a result of too-high amplitude streaks that become unstable. Case C4, with an even higher streak amplitude than C3, transitions earlier than C3. Interestingly, however, C4 has a stronger stabilizing effect than C2 on TS waves due to the higher streak amplitude, but C2, with more stable streaky base flow, is a better configuration for transition delay.

The observation that the streak amplitude is a delicate quantity is in agreement with results from Shahinfar *et al.* (2013), where it was shown that an optimum exists. Below the optimum, the streaks are not sufficiently strong to attenuate the TS waves effectively and above it, the high-amplitude streaks can become unstable. However, their suggested streak amplitude optimum is 30 % (for wall-mounted MVGs), whereas the current data suggest a value of approximately 50 % for FSVGs. This was already discussed in § 4.2. In [figure 8\(b\)](#), the success of the control can be quantified by comparing C1 with the reference case at $x \approx 515$ mm. With the FSVGs, the disturbance level stays essentially constant down to approximately $x = 250$ mm, whereafter it starts decaying until approximately $x = 515$ mm. At this downstream location, the disturbance level for C1 is approximately 17 times smaller than in the reference case. Comparing the onset of transition for the reference case at $x = 400$ mm, one can estimate the transition delay to be at least 40 % by extrapolating the disturbance growth curve for C1 to the same level as the reference case at $x = 400$ mm, taking the distance from the virtual origin at $x \approx -215$ mm (cf. [figure 8\(b\)](#)).

As the measurement region is not long enough to fully cover the transitional region for the controlled cases, another way to present the transition delay achieved with the FSVGs can be employed. [Figure 9](#) also shows E^{int} , but at a fixed streamwise location while the voltage provided to the loudspeaker is gradually increased. The measurement was performed at the most downstream location ($x = 596$ mm) in the boundary layer, and results are shown for the two most successful cases from [figure 8](#), namely C1 and C3, and compared to the uncontrolled case. Note that the speaker voltage is a set-up-dependent variable, as different speakers and different tubing connections will affect the generated perturbations. Both controlled cases show a stabilization of the boundary

layer compared to the reference case by exhibiting the abrupt increase in E^{int} , associated with transition onset, at considerably higher voltages fed to the loudspeaker. It can be seen that in agreement with the previous results, C1 is able to stabilize the flow most successfully, making the controlled boundary layer over 110 % more persistent to the imposed disturbances (in terms of loudspeaker voltage, 1.5 V / 0.7 V at onset) compared to the reference case. One can observe that the onset of transition between the two controlled cases, C1 and C3, takes place at an almost equal voltage. What makes C1 more successful over C2 here is the lower growth rate of E^{int} with increasing disturbance amplitudes. The slightly scattered data can be attributed to unconverged measurements in the highly intermittent transitional flow.

5. Conclusions

In this experimental study, we demonstrate that free-stream vortex generators (FSVGs) can successfully generate a streaky base flow, with alternating high- and low-speed regions, which is capable of delaying the transition from laminar to turbulent flow in a boundary layer. The aim of using these free-stream devices is to minimize the unstable wake effect inside the boundary layer caused by the physical presence of wall-mounted miniature vortex generators (MVGs) and their initially relatively strong vortices, leading to sharp mean velocity gradients in both the wall-normal and spanwise directions.

After a limited but feasible FSVG parameter variation study consisting of five different cases (C0–C4), we were able to find a case that, in the range of the current investigation, optimizes the stabilizing effect on the boundary layer. Notably, a balance between too-weak streaks, which have insufficient effect on the transition, and streaks with a too-large amplitude, which can develop instabilities, was achieved. The most successful configuration significantly attenuated Tollmien–Schlichting waves by 80 %, and led to a delay in transition location of approximately 40 %.

Results indicate that the optimal streak amplitude when generated through free-stream vortices is considerably higher as compared to previous studies that employed devices mounted on the surface with vortices generated inside the boundary layer. This can be linked to the fact that in the present case, the geometry disturbing the boundary layer is minimal. Previous studies have shown that MVGs feature an absolute instability in their wake, which is avoided (or at least significantly reduced) using FSVGs. Another explanation is that the streaks generated by FSVGs and MVGs are different and not directly comparable. From the present results, one can see that the maximum boundary layer modulation takes place further away from the wall with FSVGs compared to MVGs, which leads to weaker mean velocity gradients. For further analysis, a direct comparison between the two different types of vortex generators would be necessary. This would indicate if the significantly higher streak amplitudes behind FSVGs actually lead to improved transition delay compared to MVGs, or if the stabilization actually is weaker since the base flow modulation is not as strong close to the wall where the largest production of turbulence kinetic energy takes place.

The experimental results aim to validate predictions and numerical simulations from prior studies on transition delay using free-stream vortices, emphasizing the efficacy of passive, energy-efficient solutions in aerodynamic applications. Future work may explore the scalability of this approach in practical engineering systems, such as aircraft fuselages, to maximize the benefits in reducing skin-friction drag and improving overall efficiency. Moreover, FSVGs may have potential in delaying other boundary layer transition mechanisms, such as free-stream turbulence induced transition, due to the low initial disturbance amplification.

Declaration of interests The authors report no conflict of interest.

Appendix A. Comparison to Siconolfi *et al.* (2015b) data

In the study by Siconolfi *et al.* (2015b), DNS of a Blasius boundary layer with artificial vortices placed in the free stream were performed. In their DNS, they showed boundary layer streak formation, as the vortices interacted with the boundary layer, which was able to delay the transition to turbulence. Direct comparison with the results of the present study is impossible, however, since several parameters differ. For the most efficient case to delay transition in the simulation, the vortices are introduced at $x_v = 52$ mm, i.e. further upstream with respect to the present experiment where the FSVG array is placed at $x_v = 210$ mm (with the virtual origin taken into account.) In addition, the vortices are introduced at a different height in the DNS, featuring $h_v = 3.9$ mm ($h_v/\delta_{99} = 2.5$), which is related to the fact that the boundary layer is relatively thin at the considered downstream location. Finally, the free-stream speeds are different. In the DNS, $U_\infty = 7.7$ m s⁻¹ while in the experiment, $U_\infty = 5.9$ m s⁻¹. This speed difference influences the vortex circulation, which cannot be measured in our experimental study using only a single hot wire. This quantity also strongly depends on the angle of attack of the delta wings α . It is worth pointing out that in the DNS, there will never be a wake effect as in the experiment since there is no physical wing present.

Regardless of these disparities, a qualitative comparison of the streak amplitude can be attempted. Since Siconolfi *et al.* (2015b) utilized a maximum-based definition of the streak amplitude, the same quantity was calculated for the present data:

$$A_{ST}^{max}(x) = \max_y \left[\max_z \{U(x, y, z)\} - \min_z \{U(x, y, z)\} \right] / (2U_\infty). \quad (A1)$$

Note that, as mentioned before, this quantity does not contain a spanwise length scale, which might be misleading when comparing different cases. However, the spanwise periodic window is the same in all cases in both studies, meaning that the absolute values are, in fact, comparable.

Results for the experimental cases C1–C4, as well as the two final cases from the DNS, featuring different vortex strengths (E1 and E2), are shown in figure 10.

The figure shows that both the absolute values and the overall shape of the streak amplitude evolution agree reasonably well. When compared to wall-mounted MVGs, which were employed in numerous previous studies (e.g. Shahinfar *et al.* 2012, 2013; Sattarzadeh *et al.* 2014), the streaks grow more slowly and are sustained longer in the flow. For these devices, the streak amplitude maximum is usually reached after approximately 200 mm, and it decays rather quickly. This is likely due to the viscous dissipation of the generated vortices, which is stronger close to the wall. Although in the current study the maximum A_{ST} cannot be resolved due to limitations in the traversing length, case C2 seems to agree with E2, and C1 and C3 are in the same range as E1. Case C4 clearly reaches a streak amplitude that is too high for successful control.

In the DNS study, case E2 was judged as the best result, featuring damping of the imposed TS waves while the streaks were weak enough not to cause instabilities in the flow. Case E1 was still able to delay the transition, but exhibited an unstable region further downstream. The present experiment shows that C1 has the best stabilization effect on the boundary layer, which features a higher streak amplitude than E2, but still less than E1. Interestingly, the identified best cases in the experiment and from the DNS have approximately the same streak amplitude and approximately the same streamwise streak amplitude evolution.

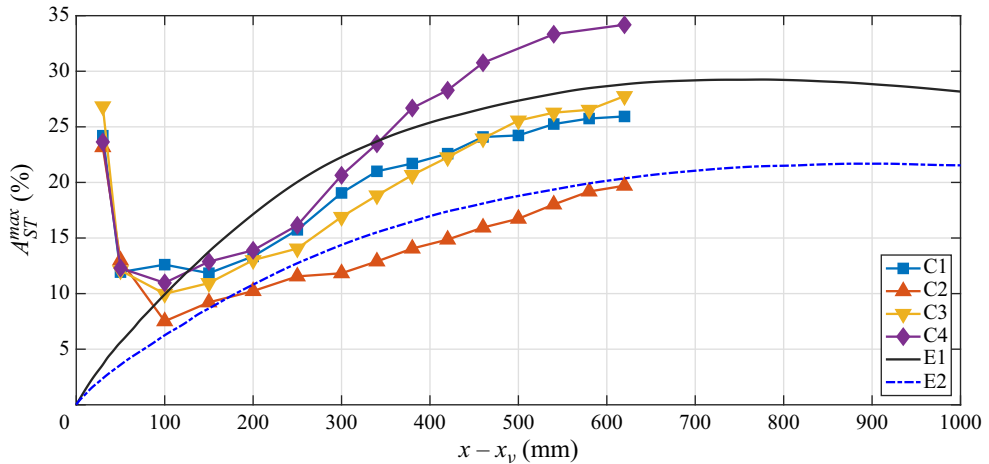


Figure 10. Comparison of the streak amplitude max measure from the experiment with the DNS study by Siconolfi *et al.* (2015b) (cases E1 and E2).

REFERENCES

- ANDERSSON, P., BRANDT, L., BOTTARO, A. & HENNINGSON, D.S. 2001 On the breakdown of boundary layer streaks. *J. Fluid Mech.* **428**, 29–60.
- BAKCHINOV, A.A., GREK, G.R., KLINGMANN, B.G.B. & KOZLOV, V.V. 1995 Transition experiments in a boundary layer with embedded streamwise vortices. *Phys. Fluids* **7** (4), 820–832.
- BARCKMANN, K., TROPEA, C. & GRUNDMANN, S. 2015 Attenuation of Tollmien–Schlichting waves using plasma actuator vortex generators. *AIAA J.* **53** (5), 1384–1388.
- COSSU, C. & BRANDT, L. 2002 Stabilization of Tollmien–Schlichting waves by finite amplitude optimal streaks in the Blasius boundary layer. *Phys. Fluids* **14** (8), L57–L60.
- COSSU, C. & BRANDT, L. 2004 On Tollmien–Schlichting-like waves in streaky boundary layers. *Eur. J. Mech. B/Fluids* **23** (6), 815–833.
- CUI, Z. 2023 Modulation of the laminar boundary layer using free-stream vortices. Master’s thesis, KTH Royal Institute of Technology.
- DOWNS, R.S., FALLENIOUS, B.E.G., FRANSSON, J.H.M. & MÄRTENSSON, H. 2017 Miniature vortex generators for flow control in Falkner–Skan boundary layers. *AIAA J.* **55** (2), 352–364.
- DOWNS, R.S. & FRANSSON, J.H.M. 2014 Tollmien–Schlichting wave growth over spanwise-periodic surface patterns. *J. Fluid Mech.* **754**, 39–74.
- FRANSSON, J.H.M., BRANDT, L., TALAMELLI, A. & COSSU, C. 2004 Experimental and theoretical investigation of the nonmodal growth of steady streaks in a flat plate boundary layer. *Phys. Fluids* **16** (10), 3627–3638.
- FRANSSON, J.H.M., BRANDT, L., TALAMELLI, A. & COSSU, C. 2005 Experimental study of the stabilization of Tollmien–Schlichting waves by finite amplitude streaks. *Phys. Fluids* **17** (5), 054110.
- FRANSSON, J.H.M. & TALAMELLI, A. 2012 On the generation of steady streamwise streaks in flat-plate boundary layers. *J. Fluid Mech.* **698**, 211–234.
- FRANSSON, J.H.M., TALAMELLI, A., BRANDT, L. & COSSU, C. 2006 Delaying transition to turbulence by a passive mechanism. *Phys. Rev. Lett.* **96** (6), 064501.
- KACHANOV, I.S. & TARARYKIN, O.I. 1987 An experimental study of the stability of a relaxing boundary layer. *Proc. Siberian Div. USSR Acad. Sci. Ser. Tech. Sci.* **18** (5), 9–19, in Russian.
- LINDGREN, B. & JOHANSSON, A.V. 2002 Evaluation of a new wind tunnel with expanding corners. Tech. Rep. TRITA-MEK 2002: 14. KTH Royal Institute of Technology.
- LOISEAU, J.-C., ROBINET, J.-C., CHERUBINI, S. & LERICHE, E. 2014 Investigation of the roughness-induced transition: global stability analyses and direct numerical simulations. *J. Fluid Mech.* **760**, 175–211.
- LOZANO, F. 2017 On the use of miniaturized delta wings to modulate the Blasius boundary layer. Master’s thesis, KTH Royal Institute of Technology, diva2:1140141.
- MARTÍN, J.A. & PAREDES, P. 2017 Three-dimensional instability analysis of boundary layers perturbed by streamwise vortices. *Theor. Comput. Fluid Dyn.* **31** (5–6), 505–517.

- MUTHURAMALINGAM, M., PUCKERT, D.K., RIST, U. & BRUECKER, C. 2020 Transition delay using biomimetic fish scale arrays. *Sci. Rep.* **10** (1), 1–13.
- POPE, S.B. 2000 *Turbulent Flows*. Cambridge University Press.
- RÖMER, T.M., SCHULZ, K.A., WU, Y., WENZEL, C. & RIST, U. 2023 Delay of laminar–turbulent transition by counter-rotating cylindrical roughness elements in a laminar flat plate boundary layer. *Exp. Fluids* **64** (2), 42.
- SATTARZADEH, S.S. & FRANSSON, J.H.M. 2014 Experimental investigation on the steady and unsteady disturbances in a flat plate boundary layer. *Phys. Fluids* **26** (12), 124103.
- SATTARZADEH, S.S. & FRANSSON, J.H.M. 2015 On the scaling of streamwise streaks and their efficiency to attenuate Tollmien–Schlichting waves. *Exp. Fluids* **56** (3), 1–16.
- SATTARZADEH, S.S. & FRANSSON, J.H.M. 2016 Mastering nonlinear flow dynamics for laminar flow control. *Phys. Rev. E* **94** (2), 021103.
- SATTARZADEH, S.S. & FRANSSON, J.H.M. 2017 Spanwise boundary layer modulations using finite discrete suction for transition delay. *Exp. Fluids* **58** (3), 14.
- SATTARZADEH, S.S., FRANSSON, J.H.M., TALAMELLI, A. & FALLENIOUS, B.E.G. 2014 Consecutive turbulence transition delay with reinforced passive control. *Phys. Rev. E* **89** (6), 061001.
- SCHLICHTING, H. 1933 Zur Entstehung der Turbulenz bei der Plattenströmung. *Nachr. Ges. Wiss. Göttingen, Math.-Phys. Kl.* 181–208; *Z. Angew. Math. Mech.* **13**, 171–174.
- SCHUBAUER, G.B. & SKRAMSTAD, H.K. 1947 Laminar boundary-layer oscillations and stability of laminar flow. *J. Astronaut. Sci.* **14** (2), 69–78. arXiv: <https://doi.org/10.2514/8.1267>.
- SHAHINFAR, S., FRANSSON, J.H.M., SATTARZADEH, S.S. & TALAMELLI, A. 2013 Scaling of streamwise boundary layer streaks and their ability to reduce skin-friction drag. *J. Fluid Mech.* **733**, 1–32.
- SHAHINFAR, S., SATTARZADEH, S.S., FRANSSON, J.H.M. & TALAMELLI, A. 2012 Revival of classical vortex generators now for transition delay. *Phys. Rev. Lett.* **109** (7), 074501.
- SICONOLFI, L., CAMARRI, S. & FRANSSON, J.H.M. 2015a Boundary layer stabilization using free-stream vortices. *J. Fluid Mech.* **764**, R2.
- SICONOLFI, L., CAMARRI, S. & FRANSSON, J.H.M. 2015b Stability analysis of boundary layers controlled by miniature vortex generators. *J. Fluid Mech.* **784**, 596–618.
- SZABÓ, A., NAGY, P.T., DE BAETS, G., VANIERSCHOT, M. & PAÁL, G. 2024 Stability analysis of a streaky boundary layer generated by miniature vortex generators. *Comput. Fluids* **269**, 106123.
- TANI, I. & KOMODA, H. 1962 Boundary-layer transition in the presence of streamwise vortices. *J. Aerosp. Sci.* **29** (4), 440–444.
- TOLLMIEEN, W. 1929 Über die Entstehung der Turbulenz. *Nachr. Ges. Wiss. Göttingen, Math.-Phys. Kl.* 21–44.
- WEINGÄRTNER, A. 2024 Experimental studies of laminar boundary layers: instability, transition and control. *PhD thesis*, KTH Royal Institute of Technology.
- WEINGÄRTNER, A., MAMIDALA, S.B. & FRANSSON, J.H.M. 2023a Instabilities in the wake of an isolated cylindrical roughness element. *J. Fluid Mech.* **960**, A8.
- WEINGÄRTNER, A., MAMIDALA, S.B. & FRANSSON, J.H.M. 2023b Application of miniature vortex generators for boundary layer transition delay. In *AIAA SCITECH Forum*, AIAA-2023-0097. Published Online, 19 Jan. 2023. <https://doi.org/10.2514/6.2023-0097>